Determining the Effective Permeability of a Laminated CoZrTaB (CZTB) film, through Consideration of Demagnetisation Effects and Eddy-Displacement Currents

Ruaidhrí Murphy[1], Guannan Wei[1], Ansar Masood[1], Cian O'Mathúna[1], Zoran Pavlovic[1], Paul McCloskey[1], and Séamus O'Driscoll[1]

[1]Tyndall National Institute, University College Cork, Ireland

Multi-laminated thin film inductors are a key emerging technology to enable highly integrated, on-chip, voltage regulators. The permeability of a magnetic core at high frequency is a key determiner of inductance density. In this paper, a multi-lamination magnetic core made up of alternate CZTB amorphous, uniaxially anisotropic magnetic films and AlN dielectric layers is investigated. The individual films are approximately 200 nm thick, appropriate for operation at over 100 MHz, but the laminated structure and overall thickness of several micrometres mean that analytical methods are impractical for computing demagnetisation. Magnetostatic Finite Element Analysis (FEA) is used to model the magnetic core demagnetisation, accounting for various length/width dimensions, magnetic film thicknesses and dielectric thicknesses. At higher frequencies, the dielectric layers, which are included in the structure to suppress induced eddy-currents allow displacement currents to flow through the dielectric layers and lead to increased eddy currents circulating around the overall core structure and thus further increasing loss and reducing permeability. Eddy-current FEA simulations which include the displacement currents, and an analytically derived Equivalent Circuit Model (ECM) are used to model the real and imaginary (loss) components of permeability spectra. The work, therefore determines the combined contributions of both demagnetisation effects and eddy-displacement currents to the reductions in real permeability and the increase in loss components for thicker multi-laminated magnetic cores. Permeameter measurements on fabricated cores, having ten laminations, and with various AlN thicknesses (10, 20, 40 and 60 nm) gave excellent agreement with the predicted effective permeability through the approach of combining the FEA and ECM models, over the 10 MHz to 1 GHz frequency range. It was shown, that at 100 MHz, for multi-laminated cores with thin or higher k dielectric layers, that displacement-eddy currents are dominant, giving a power loss an order of magnitude higher than would be for magnetically induced eddy currents alone.

***Index Terms*—Thin-film magnetic, CZTB, multi-laminated, AlN, dielectric layer, displacement-eddy, demagnetisation, effective permeability, inductor-on-silicon, magnetic skin effect, integrated voltage regulator.**

I. Introduction

Advanced high frequency voltage regulators are emerging which use inductor devices having magnetic cores consisting of multiple laminations of thin film magnetic material with alternating insulating (dielectric) layers to increase the magnetic device density, for high frequency application, by allowing increased cross-sectional area of magnetic material while preventing excess eddy currents in the magnetic core [1], [2], [3], [4]. However, at very high switching frequencies, the dielectric layers' (capacitive) impedance reduces, so that the lamination effectiveness reduces as displacement currents flow through the insulating layers. These displacement-eddy currents both increase the power loss and reduce the effective permeability of the laminated core. The effective permeability, μ_{eff}, is the permeability of a sample after demagnetisation and displacement-eddy current effects have been accounted for. By increasing the number of laminations and dielectric thickness, an inductor with a high inductance density, capable of operating at higher frequencies, can be fabricated.

The drive towards higher inductance density makes having a thicker cross-sectional area of core desirable. For very thin films where the film thickness is very small compared to the width and the length, the thin film approximation is usually made, whereby the demagnetisation factor can be assumed to equal zero, along the in-plane axes [5]. However, this assumption is not correct if the thickness of the thin film is sufficiently high or if there are multiple laminations of thin films that are sufficiently close together.

The demagnetisation factor of a magnetic core is dependent on its geometry and permeability. For an elliptical core the demagnetisation factor can be calculated accurately, as the fields inside the core are uniform, and there is no dependence on permeability [6], [7]. For non-elliptical shapes, the demagnetisation factor may be calculated numerically but certain approximations must be made, such as averaging of field intensities, in the material. Examples of analytical methods are presented by Aharoni [8], calculating the demagnetisation factor of a general rectangular prism, and by Parker [9]. These methods are dimension dependent and are subject to errors [10]. Similarly, these methods do not work when the case of a multi-laminated structure, in which the layers are close together, is considered. A method is developed in [10], whereby the demagnetisation factor is determined numerically using electromagnetic field simulation. The paper shows a good matchup between simulated and experimental demagnetisation factors. This simulation method can be applied to magnetic material with an arbitrary shape, with various values of material susceptibility (permeability) and with multiple laminations.

Recognizing the difficulty of analytically calculating the demagnetisation for multi-domain and laminated magnetic films, [11] presents a post-processing methodology for use with an FEA simulator to separately compute the demagnetisation factors, in each axis, for multi-laminated thin film cores. The post-processing method is developed to calculate the demagnetisation factor along the easy-axis, taking into account the edge-curling wall of laminated magnetic films, to compute the FMR using the Kittel equation. We use equations (2) – (4) from [11], in similar fashion, to compute the demagnetisation factor along the hard-axis by using averaged volume integrals of applied field, internal magnetic field and magnetization fields as simulated by a 3-D magnetostatic solver. There is no net reduction in demagnetisation along the hard-axis due to edge-curling [11].

Charles Sullivan et al., [12], performs a 2-D simulation of both eddy and displacement currents to compute high frequency loss in a multi-laminated film. Our paper similarly uses a 2-D model of a multi-laminated film to compute loss, but additionally includes the reduction in real permeability, and incorporates the shape demagnetisation effects from the magnetostatic simulations. We separate out the impacts of eddy, displacement-eddy and demagnetisation on the permeability spectra. We are therefore able to independently assess all of the mechanisms which contribute to the effective permeability and loss spectra on the multi-laminated thin-film core, excepting the ferromagnetic resonance (FMR) effects. Treatment of FMR effects are outside the scope of this work and are explained in works such as [13].

A magnetic core system consisting of multiple thin layers of CZTB and AlN is modelled. The AlN layers act as insulators between the layers of CZTB to suppress eddy currents. But at high frequencies displacement currents flow through the AlN and the system begins to behave as a single equivalently thick core with circulating eddy currents. The effect of the thickness of the AlN is investigated to assess the effectiveness of thicker dielectric layers in suppressing displacement-eddy currents. A discrete ECM using coupled Maxwell equations in integral form was developed by [14] to model the magnetic response of thin laminae including the effects of displacement currents. The ECM is further used by Geri et al. [15] and improved with the addition of the resistance parameter along the z-axis, as per Figure 1, of the laminates.

We use this ECM to compute displacement-eddy currents and their effects on system quality factor, Q, for various AlN dielectric thicknesses. Finally, simulation and ECM results are compared to experimental measurements of laminations of uniaxial anisotropic CZTB and AlN films, which were sputtered on a silicon substrate. Experimental data from Permeameter measurements, on samples comprising of 10 laminations of 200 nm CZTB alternating with 10 laminations of AlN at various thicknesses (10,20,40 and 60 nm) and to 1 GHz.

II. Demagnetisation Factor for A Single Thin Film

The demagnetisation factor of a magnetic material core is dependent on the shape of the core. The demagnetisation field of the core is the magnetization of core multiplied by the demagnetisation factor [16].

The demagnetisation factor of a single thin film of CZTB has been calculated using the FEM tool Ansys Maxwell, a 3-D model of the film and the simulation method of [11]. An applied external magnetic field was imposed, and the internal magnetic field and magnetic flux density were simulated. The simulation was conducted magnetostatically to avoid eddy or displacement currents, so that the demagnetisation factor could be isolated. Table 1 shows the difference in the computed demagnetisation factor for the method, versus other calculation methods for the same sample. This trial with equal length and width would be expected to have high demagnetisation.

Along the applied field (x-axis) the following formula was used to calculate the demagnetisation factor and the apparent real part of permeability:

The magnetization,

$$M_x = \chi H_{in_x} \tag{1}$$

where M_x is the magnetization, χ is the susceptibility of the bulk material and H_{in_x} is the internal magnetic field strength. The bulk material relative permeability of CZTB is set equal to 550, based on our typical sputtering process run.

The average magnetisation may be determined as follows:

$$M_{x_{avg}} = \frac{1}{V_{core}} \int M_x dV_{core} \tag{2}$$

where V_{core} is the volume of the magnetic core. The internal magnetic field strength,

$$H_{in_{x_{avg}}} = \frac{1}{V_{core}} \int H_{in_x} dV_{core} \tag{3}$$

$$N_x = \frac{H_{apl} - H_{in_{x_{avg}}}}{M_{x_{avg}}} \tag{4}$$

where N_x is the demagnetisation factor and H_{apl} is the external applied magnetic field strength. The apparent permeability is permeability the core would exhibit in an inductor device and is calculated as follows:

$$\mu_{\text{app}} = \langle \mu_{app_x} \rangle = \frac{\langle B_x \rangle}{\mu_0 H_{apl}} \tag{5}$$

Where μ_{app} ($\langle \mu_{app_x} \rangle$) is the apparent permeability (averaged magnetostatic) as determined by simulation and B_x is the magnetic flux density in the core [17]. The DC relative permeability of the core,

$$\mu_r = \frac{\langle \mu_{app_x} \rangle - N_x \langle \mu_{app_x} \rangle}{1 - N_x \langle \mu_{app_x} \rangle} \tag{6}$$

where μ_r is the DC relative permeability of the core.

This article has been accepted for publication in IEEE Transactions on Magnetics. This is the author's version which has not been fully edited and content may change prior to final publication. Citation information: DOI 10.1109/TMAG.2024.3494675

Table 1. Static demagnetisation methods and calculations for a 500 μm × 500 μm & 1 μm thick CZTB core.

Ref	[8]	[18]	This work
Method	Analytical equation for a rectangular general prism	Thin film assumption based on the aspect ratio	Extraction of demagnetisation factor from an FEM simulation
N_x	0.0044	0.002	4.17E-04

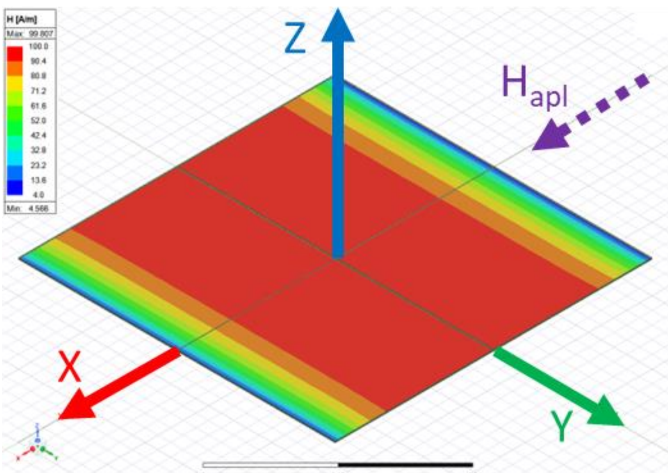

Figure 1. 3D simulation of demagnetisation of a thin film, 2000 nm thick, with magnetic field strength plotted.

Figure 1 and Figure 2 show the magnetic field strength inside the core and the expected demagnetisation profile. As can be seen, the magnetic field strength is greatest at the center of the laminated core and weaker at the edges normal to the direction of the applied field.

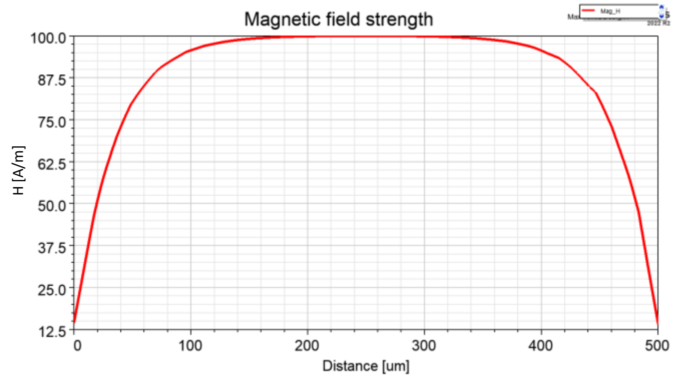

Figure 2. Magnetic field strength along the direction of magnetization inside a single thin film of CZTB at 0 Hz.

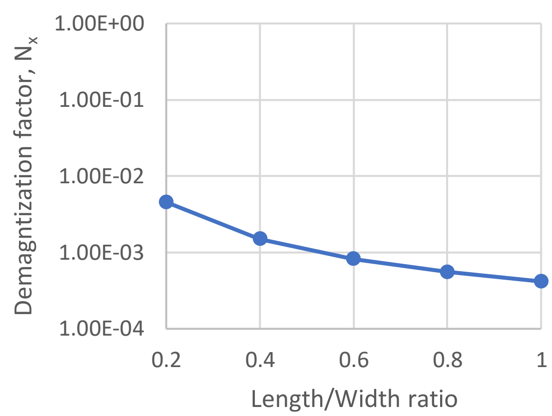

Figure 3. N_x for various Length/Width ratios. CZTB film of Width 500 μm and thickness 1 μm.

The ratio of the length of the lamination to the width is important in determining the demagnetisation factor. For a fixed width, see Figure 3, increasing the length of a CZTB lamination will decrease the demagnetisation factor resulting in a magnetic core with an apparent permeability closer to the intrinsic permeability of the material. In contrast, increasing the core thickness increases the demagnetisation factor. Figure 4 shows that for a very thin lamination the demagnetisation factor is negligibly small. A sample with a very small demagnetisation factor will result in a measured apparent permeability very close to the material's intrinsic permeability. As the thickness is increased apparent permeability drops.

This article has been accepted for publication in IEEE Transactions on Magnetics. This is the author's version which has not been fully edited and content may change prior to final publication. Citation information: DOI 10.1109/TMAG.2024.3494675

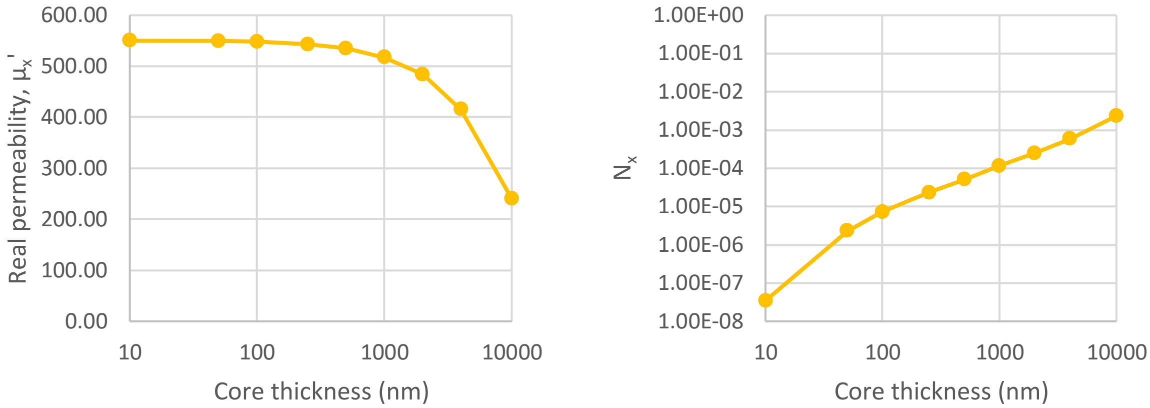

Figure 4. μ_x' and N_x (demagnetisation) for a single CZTB core (500 μm × 500 μm) versus thickness.

III. Demagnetisation Factor for a Laminated Core with Multiple Layers of Thin Films

Multiple laminations of CZTB and AlN are stacked to increase the overall cross-sectional area of magnetic material, while suppressing high frequency eddy currents, see Figure 5. The magnetostatic FEA solver simulates the laminated structure, in a similar manner to that in Section II, to determine the overall demagnetisation factor. Separating the CZTB laminations, with AlN dielectric laminations, results in a lower demagnetisation factor when compared to a single thick lamination of equivalent thickness to the sum of, in this case, eight laminations of CZTB and AlN. Increasing the spacing between CZTB films, equivalent to increasing the thickness of the AlN films, increases the demagnetisation factor, because adjacent films perform less mutual counteraction of each other's demagnetisation fields. This effect is similar to increasing the thickness of a single equivalently thick lamination. Eventually a point is reached whereby permeability begins to increase. This occurs when the distance between laminations is large enough for them to become isolated magnetically and be equivalent to single thin films. Increasing the total thickness of the magnetic core alters the demagnetisation factor as seen in Figure 7.

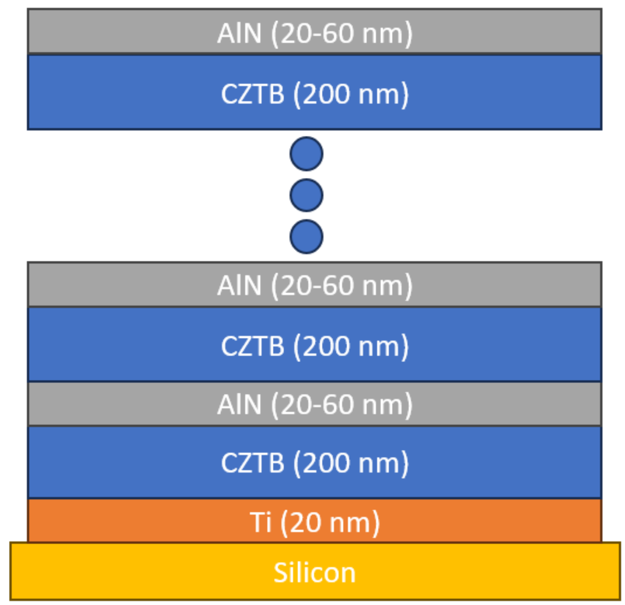

Figure 5. Cross-sectional view of a multi-laminated CZTB and AlN core. Experimental work was done using 10 laminations of 200 nm thick CZTB. Analysis of demagnetisation in multi-lamination CZTB was done for 8 laminations of CZTB films of 250 nm thickness.

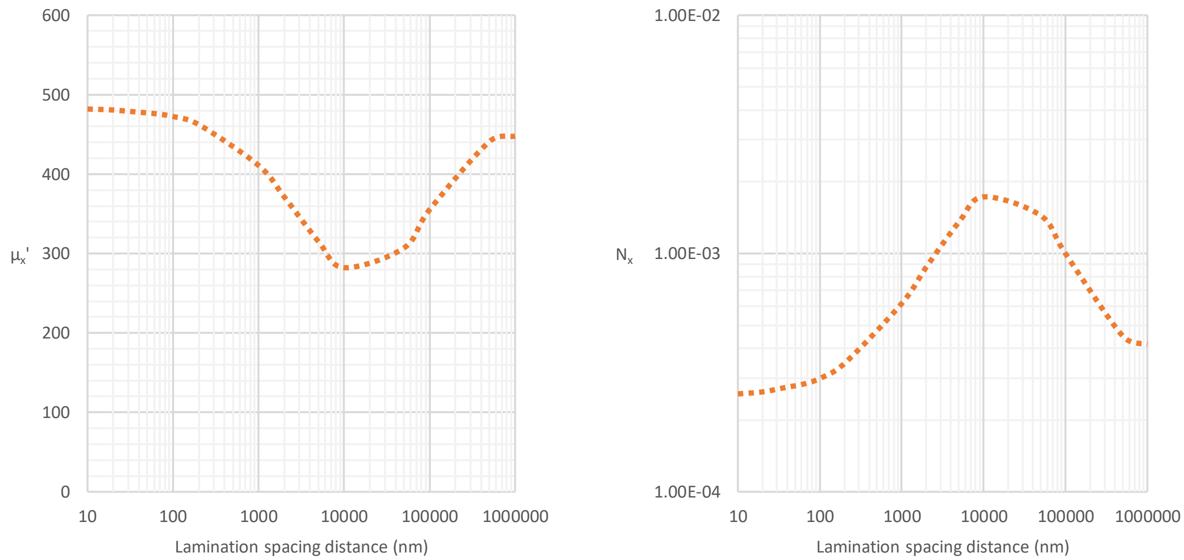

Figure 6. μ_x' & N_x vs lamination spacing distance for 8 CZTB laminations with 500µm width and 500µm length at an applied magnetic field strength of 100 A/m.

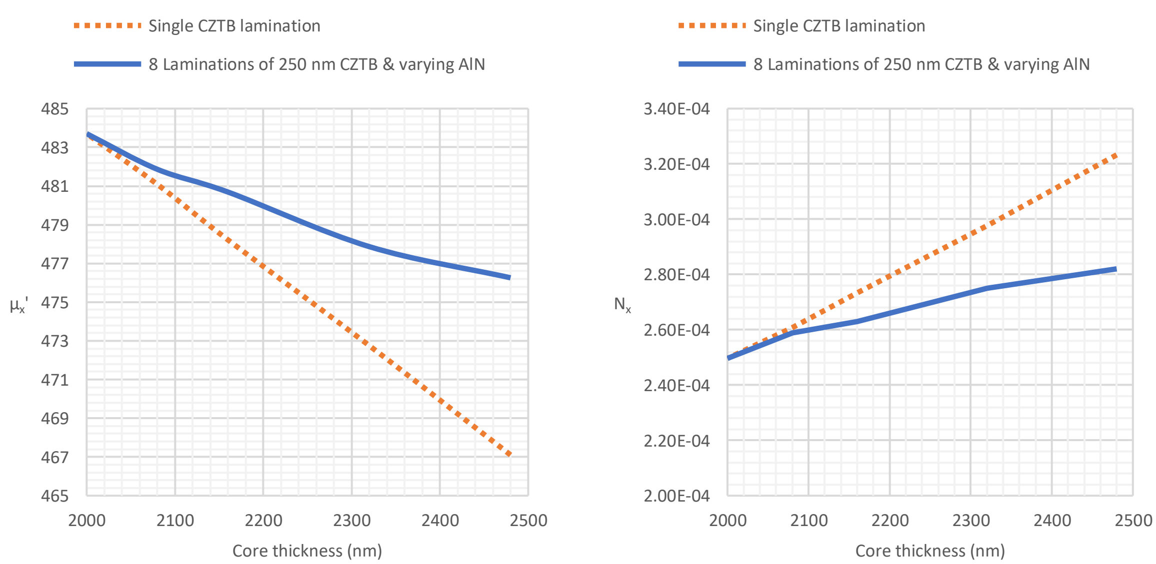

Figure 7. μ_x' & N_x vs core thickness for a single CZTB lamination and a core with 8 laminations of constant 250 nm thick CZTB with various AlN thicknesses (0 to 60 nm) at an applied magnetic field strength of 100 A/m.

IV. Eddy And Displacement Current Effects In Multiple Thin Film Laminations

At high frequencies, eddy current density increases in a magnetic core. The eddy currents circulate creating a magnetic field that opposes the external field and causes increased flux densities in outer regions, as a magnetic skin effect. The increased eddy currents and lower internal fluxes generate more power loss and a decrease in the effective real permeability. Higher resistivity magnetic material and multiple thinner laminations, separated by dielectric layers are used to suppress the eddy currents.

Displacement currents arise at higher frequencies when charges begin to flow through the dielectric laminations due to alternating voltage differentials induced in the magnetic lamination. At sufficiently high frequencies, the dielectric impedances reduce, so that loop current paths for induced displacement-eddy currents enlarge to cover the full cross-sectional area, with the laminations combining to behave as a single thick lamination [12]. The displacement-eddy current flows greatly increase loss.

The COMSOL eddy current simulator allows a choice to optionally include/exclude displacement currents in the simulation and this feature was used to isolate the eddy current and displacement-eddy current effects.

A. Eddy Currents Analytical Modeling

A commonly used analytical model for eddy current loss is presented in [19], and reproduced here as equation 6.

$$P_L = \frac{(2\pi f)^2 B_{peak}{}^2 A t^2}{24\rho} \tag{7}$$

Where f is frequency, B_{peak} is the peak magnetic flux density, A is the cross-sectional area, t is the thickness and ρ is the resistivity of CZTB. The formula is modified to give power loss per meter, to equate with the units given by the 2-D simulation. This represents the resistive losses in the material due to an alternating magnetic flux and can be seen in Figure 8.

B. Eddy Currents; Finite Element Analysis Modeling

Using a 2-D COMSOL FEA model, with only eddy currents enabled, it was possible to simulate the effects of eddy currents in the multi-lamination core. Due to the large width compared to the thickness of the magnetic laminations, a 2-D simulation and the independent meshing control on each axis reduces the computational demands on the computer hardware. The FEA mesh is concentrated along the x-axis with fewer mesh elements along the y-axis to improve the simulation of current paths. Demagnetisation was taken into account by setting the intrinsic real permeability of the CZTB to the apparent permeability determined from the static simulation for each AlN thickness as described in Section III. A 2-D model solves the eddy currents in the x and y axes. As can be seen in Figure 8, there is an excellent match between the simulator and the analytical model for the eddy current cross-sectional area resistive losses per unit length. When displacement currents are enabled in the simulator the loss due to eddy-displacement currents can be computed. At lower frequencies, displacement currents are insignificant, and eddy-currents are restricted to their individual laminations.

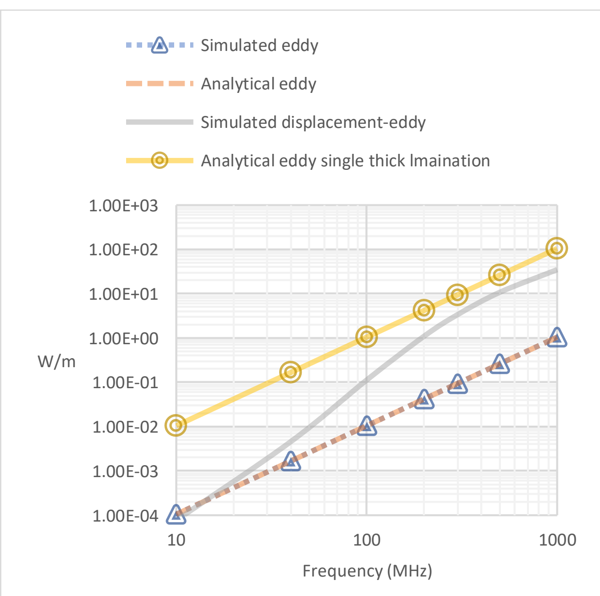

Figure 8. A comparison of cross-sectional area resistive losses per unit length, in W/m, for the analytical eddy current losses, the simulated eddy current only, losses and the simulated eddy-displacement currents for the core comprising 10 laminations of 200 nm CZTB and 60 nm AlN films of 3 mm width and 3 mm length. Also shown are the analytical eddy current losses for a single thick lamination of 2000 nm CZTB.

As the frequency increases, the displacement-eddy currents begin to dominate and the loss per unit length increases eventually approaching the eddy current only loss of an equivalently thick single lamination of the same thickness of the ten individual 200 nm CZTB laminations combined. At 100 MHz, where such cores are considered, there is an order of magnitude increase in loss per unit length when the displacement-eddy current model is compared to the eddy current models, and this applies even with relatively large AlN thickness of 60 nm. Displacement-eddy losses are the dominant loss mechanism at 100 MHz.

C. Displacement-Eddy Currents - Analytical Modeling

1) The Displacement Current Equivalent Circuit

The multi-lamination magnetic core can be represented as an equivalent electrical circuit, by using Maxwell's coupled equations in integral form [15], to model displacement-eddy currents. The equations for mesh inductance, capacitance and resistance from [14] are reproduced and have parameters defined in Table 2.

$$L = \mu_0 \mu_{app} \frac{t}{t+d} . \frac{e.t}{h}, \qquad R = \rho \frac{e}{h.t}, \qquad C = \epsilon_0 \epsilon_r \frac{e.h}{d} \tag{8}$$

Each lamination pair is represented by a mesh voltage, V_i, equal to the induced electromotive force created by the time varying magnetic field. Mesh currents are associated with mesh voltages obeying Faraday's and Ohm's law.

Table 2. Material properties and parameter values.

Parameter	Value
t, CZTB lamination thickness	200 nm
d, AlN lamination thickness	10-60 nm
e, core length perpendicular to applied field	3000 nm
h, core length parallel to applied field	3000 nm
ρ, resistivity (assumed)	150 μΩ.cm
ϵ_r, AlN relative permittivity	8.8
μ_{app}, CZTB apparent relative permeability (frequency independent)	355-425
N, number of Laminations	10

Table 2 contains the parameters values used for our multi-lamination magnetic core and with the relative permeability of the CZTB laminations after the demagnetisation factor of Section III has been taken into account. The paths of conduction and displacement currents is depicted in Figure 9 and the equivalent circuit model (ECM) of the system is depicted in Figure 10. Loop mesh analysis can be used to generate a matrix relating the induced voltage to the mesh voltages and currents. The matrix of linear equations are solved using the Gauss-

Jordan method [20]. The applied current, I_O, is proportional to the applied field, H_{app}.

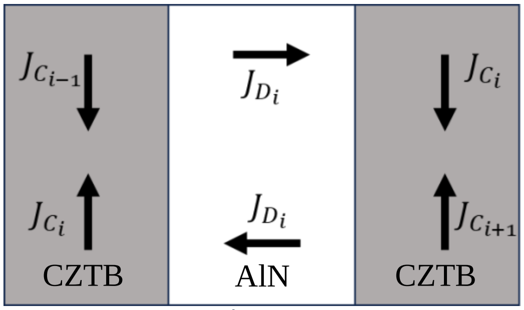

Figure 9. Cross section of the i^th film pair with conduction currents J_C and displacement currents J_D. The conduction currents are coupled to the (i±1)^th cell.

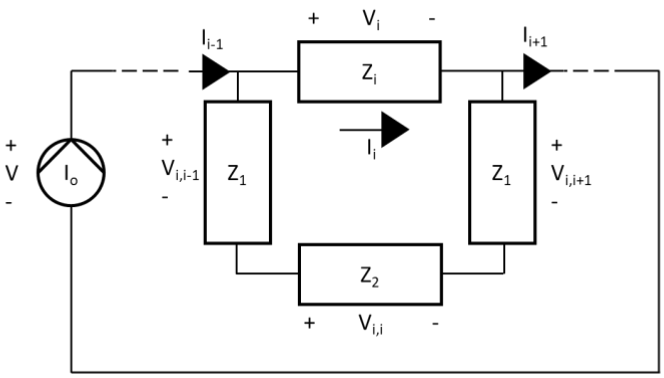

Figure 10. Equivalent circuit model for a multi-lamination magnetic core i^th film pair with displacement-eddy currents [14].

The effective real and imaginary permeabilities are found by relating the average magnetic field in each laminate to the average circuit current as in the equivalent circuit.

$$Z_i = j\omega L, \qquad Z_1 = 2R, \qquad Z_2 = \frac{4}{j\omega C} \tag{9}$$

$$\begin{pmatrix} V_1 \\ V_2 \\ \vdots \\ V_n \end{pmatrix} = \begin{pmatrix} I_1 \\ I_2 \\ \vdots \\ I_n \end{pmatrix} \begin{pmatrix} 2Z_1 + Z_2 + Z_i & -Z_1 & \cdots & 0 \\ -Z_1 & 2Z_1 + Z_2 + Z_i & -Z_1 & \cdots \\ \vdots & \vdots & \ddots & -Z_1 \\ 0 & 0 & -Z_1 & 2Z_1 + Z_2 + Z_i \end{pmatrix} \tag{10}$$

$$\frac{\langle \mu_{eff} \rangle}{\mu_{app}} = \frac{I_{lam}}{I_O} = \frac{Z^*}{Z} \tag{11}$$

where Z is the system of impedances in the absence of displacement currents and Z* is found by solving for N independent loop currents between laminate pairs as represented by the matrices in eq. 10. Z* includes the effects of the displacement currents.

Figure 8 shows that the analytical loss of an equivalent thick lamination of CZTB converges on the simulated loss per meter of the multi-lamination core, at higher frequencies.

Calculating μ' and μ'' , where μ' and μ'' are the real and imaginary parts of μ_{eff}, for magnetic cores with various AlN thicknesses allows Q to be plotted versus frequency as shown in Figure 11. As can be seen the cores with thicker AlN laminations result in higher Q-factors. Additionally, any current circulating along the z-axis is not accounted for.

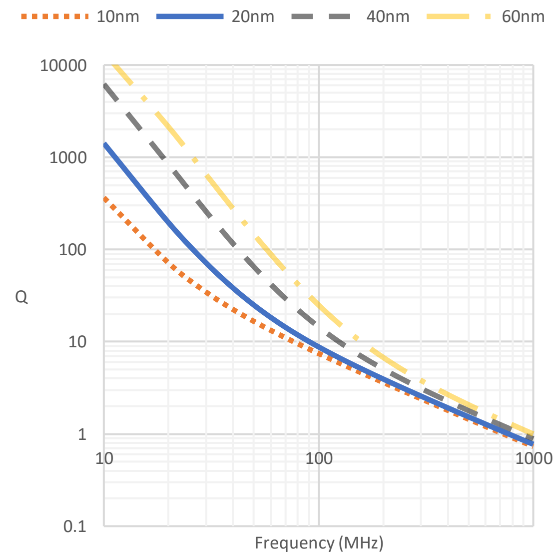

Figure 11. Analytical model plots of multi-lamination core Q vs frequency for 10, 20, 40 & 60 nm thick AlN laminations with 10 laminations of 200 nm CZTB films of 3 mm width and 3 mm length.

The analytic model is used to determine the real permeabilities for various multi-lamination core widths and a constant AlN thickness of 60 nm – shown in Figure 12 and Figure 13. The width of the core changes the inter-lamination capacitance and lamination inductance. A narrower core results in a higher resonance peak frequency due to lower inductance and capacitance values. Additionally, the resistance is highly dependent on the width of the lamination with damping depending on the resistance. A narrower core results in lower damping.

For a practical inductor, which has excitation by a winding around the core, this large outer magnetic field produced by the eddy current and displacement currents will shield the magnetic flux from the inner portion of the core cross-section. This results in a flux skin effect analogous to the skin effect in the conductors of winding [21]. This effect is not captured here, because our model applies for the case of uniform applied magnetic field along each of the laminations.

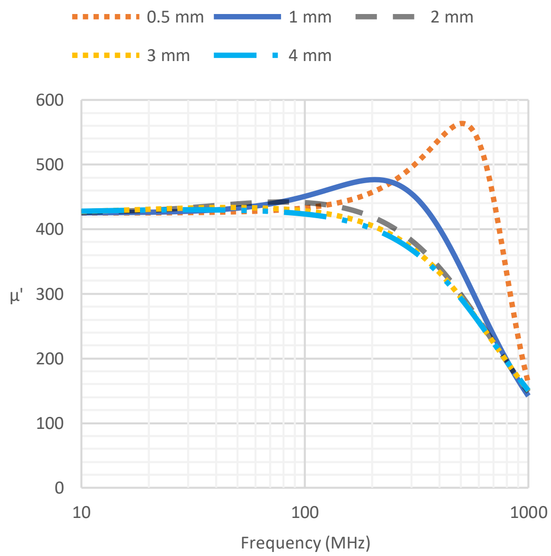

Figure 12. Analytical model plots for real permeability, μ′ vs frequency for 10 laminations of 200 nm CZTB films, with 60 nm AlN dielectrics for various widths and with constant length = 3 mm.

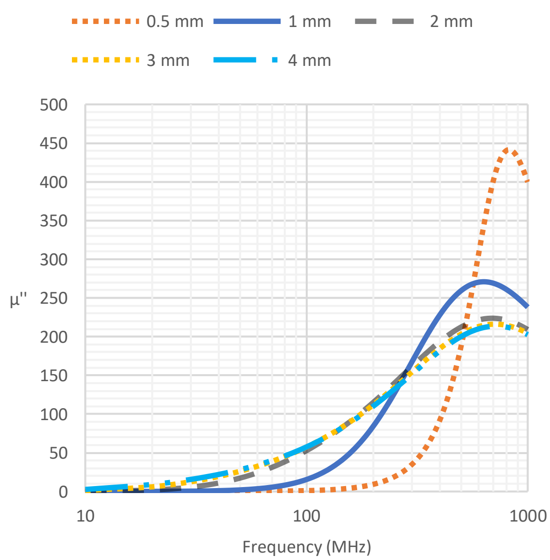

Figure 13. Analytical model plots for imaginary permeability, μ'' vs frequency for 60 nm thick AlN laminations with 10 limitations of 200 nm CZTB films for varying widths and with constant length equal to 3 mm.

.

D. Eddy Current Including Displacement Current Finite Element Modeling

The 2D COMSOL model was used with the displacement currents enabled. The dielectric layers allow the displacement-eddy currents to flow. The relative permittivity value for the magnetic material is the same as in the previous subsection. Figure 14 shows that the current densities in the lower and upper laminations are greater than the middle laminations for the 1 GHz simulation. The current densities are more equal through the laminations at 1 MHz. The flow of displacement currents redistributes the current density to be more similar to a single thick bulk magnetic lamination. Figure 8 shows the simulated loss for the multi-lamination with 60 nm thick AlN layers, approaching the analytically modeled loss for a 2000 nm thick single film of CZTB at higher frequencies.

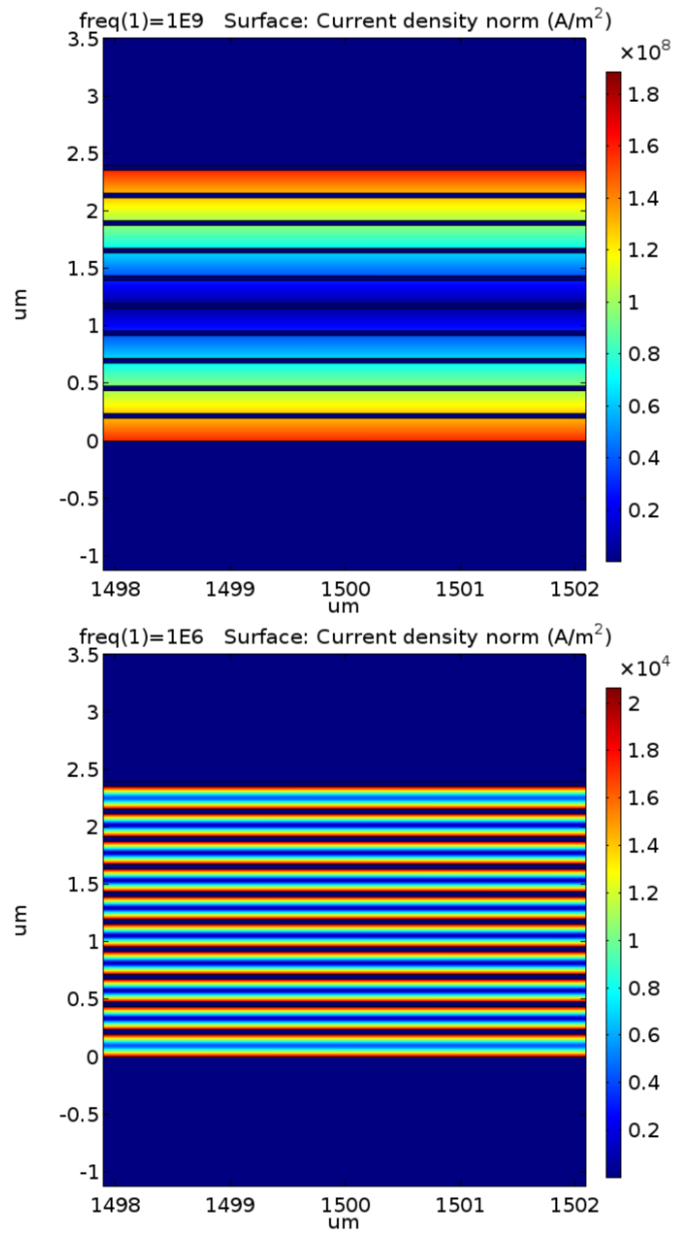

Figure 14. 2D COMSOL simulations of current distribution at 1 GHz & 1 MHz for the CZTB/AlN lamination stack with eddy and displacement currents enabled. This snapshot is at the mid-point of the lamination's width.

A consequence of these displacement currents is increased power loss and a decrease in the effective permeability due to the outer shielding field caused by the eddy currents.

In Figure 15, we studied, by varying the relative permittivity of the 60 nm AlN, the effect of displacement-eddy currents on power loss in the metallic resistivity of the CZTB laminations. It confirmed that, at 100 MHz, the displacement-eddy currents were an order of magnitude higher than eddy current only losses, for a relative permittivity of 8.8.

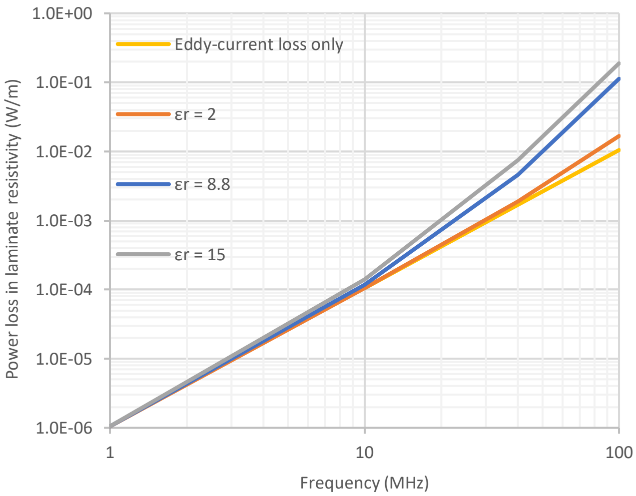

Figure 15. Simulated power loss (capturing both eddy and displacement-eddy) for various permittivity values in 60 nm dielectric laminations at an external peak magnetic field strength of 100 A/m.

V. Experimental Data For Multi-Lamination CZTB Cores

Experimental samples were fabricated on silicon using a Nordiko Advanced Energy NDX 2500-W DC-magnetron sputtering machine. A sputtering power of 500 W was used to deposit both CZTB and AlN laminations. Samples consisted of ten laminations of CZTB separated by AlN dielectric insulating layers. The samples had varying AlN lamination thickness (10, 20, 40 & 60 nm) but the same CZTB lamination thickness (200 nm), as seen in Figure 16. The samples were 3000 µm in both width and length. An uniaxial in-plane (x-axis) anisotropy with an anisotropy field value of 34 Oe was induced into the samples during sputtering through the presence of an aligning homogeneous magnetic field. Permeability was measured using a Ryowa permeameter. The real part of permeability and the quality factor are plotted versus frequency in Figure 17. A resistivity of 150 µΩ.cm was assumed for the CZTB film.

The initial (small-signal, low frequency) permeability of the samples reduces as the AlN lamination thickness increases due to demagnetisation. The permeability spectrum remains flat up to 100 MHz for each of the four different AlN thicknesses. The roll-off in permeability begins at a lower frequency for smaller AlN thickness due to the increased effect of eddy-displacement currents. The quality factor increases with the increase in the thickness of the AlN laminations. There are two distinctive changes in the slope of the quality factor versus frequency. The first change in slope is related to the onset of displacement currents flowing between laminated pairs and the second change occurs at the frequency where the displacement eddy currents are concentrated entirely in the two outermost laminations. Below 20 MHz the accuracy of the permeameter measurements is reduced due to the low resistance of the samples at lower frequencies, because of the low impedance versus the 50 Ω calibration point.

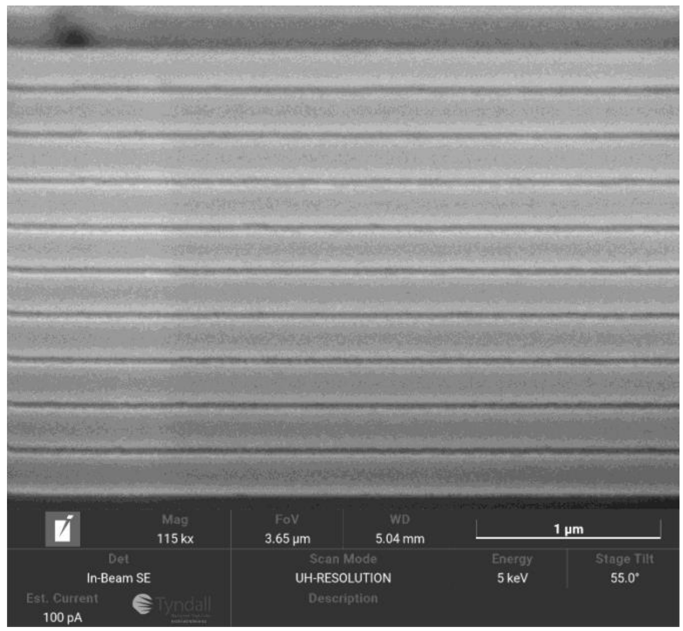

Figure 16 FIB-SEM image of the multi-lamination CZTB with AlN dielectric (40 nm) core structure, used for experimental measurements.

Non-uniformity in the AlN lamination thickness was found in some of the experimental samples after inspection with FIB-SEM imaging. Such non-uniformity can explain differences between the simulation and modeling results and the experimental data. For the case of the 60 nm AlN sample, at one cross section the AlN thickness varied from 37.7 nm to 80.3 nm with an average thickness of ~50 nm.

This article has been accepted for publication in IEEE Transactions on Magnetics. This is the author's version which has not been fully edited and content may change prior to final publication. Citation information: DOI 10.1109/TMAG.2024.3494675

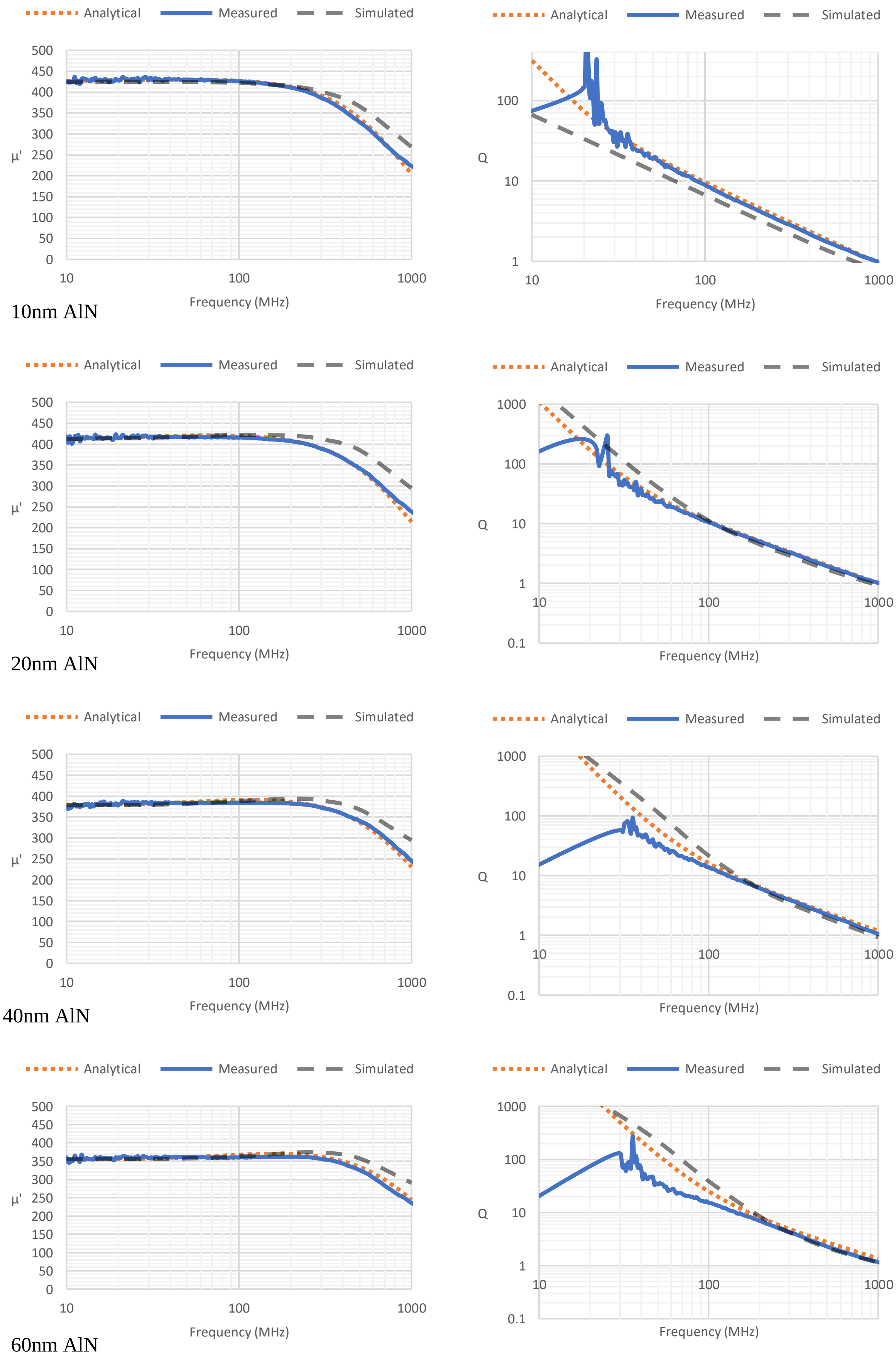

Figure 17. Analytical, measured (permeameter) & simulated μ' & Q for a multi-lamination magnetic core with 10,20,40 & 60 nm thick AlN laminations and with 10 limitations of 200 nm CZTB of 3 mm width and 3 mm length.

VI. Conclusion

For multi-laminated thin film magnetic cores the experimental and simulated results show that demagnetisation is significant and the thin-film assumption is not applicable. Static FEA modelling shows that as the thickness of the dielectric layers between the magnetic laminations is increased, the core demagnetisation factor increases.

An equivalent circuit model ECM was adopted to analytically compute μ' & μ'' across frequency and agrees well with simulated results when a low frequency μ', corrected for the effect of demagnetisation, is used as the input intrinsic material permeability. At higher frequencies, μ' begins to decrease due to increased displacement-eddy currents flowing through the laminations. Increasing the dielectric thickness reduces displacement-eddy currents, leading to a higher Q-factor but at the cost of a higher demagnetisation factor leading to a lower μ'. Reducing the width/ length ratio, was also shown to reduce the drop in μ' and increase Q due to a lower demagnetisation factor and reduced displacement-eddy current losses, because of the smaller displacement eddy current path lengths.

Multi-laminated CZTB cores with various thicknesses of AlN dielectric were fabricated and the μ' & μ'' spectra were measured using a permeameter. A good match between the analytical, experimental, and simulated results was observed. At 100 MHz, a 250% increase in the Q-factor was observed by increasing the AlN laminations from 10 nm to 60 nm. It was shown that the most significant contributor to power loss at 100 MHz and higher were displacement-eddy currents. At 100 MHz the loss from displacement-eddy currents were an order of magnitude higher than those through considering magnetically induced eddy currents alone. This result suggests that an improvement to multi-lamination CZTB magnetic cores as used in this paper would be to either increase the dielectric thickness or use a dielectric with a lower relative permittivity. The low induced eddy current loss suggests that CZTB film thickness could be substantially increased, with the production cost reducing benefit of a smaller number of laminations.

This work demonstrates the experimental validation of an efficient methodology for determining μ' & Q spectra for multi-laminated thin film magnetic cores, that incorporates static FEA modelling to determine the demagnetisation factor and the use of an ECM to determine displacement-eddy current frequency effects.

Acknowledgments

The Enterprise Ireland *LAMMAG* Innovation Partnership Program, "*High Frequency Sputtered Laminated Magnetic Cores*" (IP/2016/0479) and the *GaNonCMOS* EU Horizon 2020 project (H2020-NMBP-2016-721107) supported this research.

References

[1] C. Ó. Mathúna and S. O'Driscoll, "Heterogeneous Integration of Power Conversion using Power Supply on Chip and Power Supply in Package," 2022 24th European Conference on Power Electronics and Applications (EPE'22 ECCE Europe), Hanover, Germany, 2022, pp. 1-2.

[2] "Ultra-low loss integrated magnetics platform for high frequency power delivery networks", Pranay Podder et al., Tyndall, Chor Shu Cheng et al., Global Foundries, 11th International Conference on Integrated Power Electronic Systems; Berlin, Germany. March24-26th, 2020

[3] W. J. Lambert, M. J. Hill, K. P. O'Brien, K. Radhakrishnan and P. Fischer, "Study of Thin-Film Magnetic Inductors Applied to Integrated Voltage Regulators," in IEEE Transactions on Power Electronics, vol. 35, no. 6, pp. 6208-6220, June 2020, doi: 10.1109/TPEL.2019.2948825.

[4] P. Podder et al., "Ultra-low loss integrated magnetics platform for high frequency power delivery networks," CIPS 2020; 11th International Conference on Integrated Power Electronics Systems, Berlin, Germany, 2020, pp. 1-4.

[5] Philips Research, Prof. Holstlaan 4, 5656 AA Eindhoven, The Netherlands "High-frequency permeability of soft-magnetic Fe–Hf–O films with high resistivity", Journal of Applied Physics 83, 1569-1574 (1998) https://doi.org/10.1063/1.366867

[6] B. D. Cullity and C. D. Graham, Introduction to Magnetic Materials, 2nd ed. New York: Wiley, 2009, ISBN 978-0-471-47741-9.

[7] Journal of applied physics volume 37, number 13 December 1966 "Ballistic Demagnetizing Factor in Uniformly Magnetized Cylinders" R. 1. Joseph, Raytheon Research Division, Waltham, Massachusetts (Received 31 May 1966)

[8] Amikam Aharoni , "Demagnetizing factors for rectangular ferromagnetic prisms", Journal of Applied Physics 83, 3432-3434 (1998) https://doi.org/10.1063/1.367113

[9] R. J. Parker, Advances in Permanent Magnetism. New York: Wiley, 1990, ISBN 0-471-82293-0.

[10] Pugh, B. & Kramer, Dan & Chen, Christina. (2011). Demagnetizing Factors for Various Geometries Precisely Determined Using 3-D Electromagnetic Field Simulation. IEEE Transactions on Magnetics - IEEE TRANS MAGN. 47. 4100-4103. 10.1109/TMAG.2011.2157994.

[11] A. El-Ghazaly, R. M. White, and S. X. Wang , "Increasing ferromagnetic resonance frequency using lamination and shape", Journal of Applied Physics 117, 17E502 (2015) https://doi.org/10.1063/1.4913509

[12] Di Yao and Charles R. Sullivan , "Calculation of eddy-current loss in multilayer magnetic films considering displacement current", Journal of Applied Physics 105, 07A335 (2009) https://doi.org/10.1063/1.3074134

[13] E. van de Riet, F. Roozeboom; Ferromagnetic resonance and eddy currents in high-permeable thin films. J. Appl. Phys. 1 January 1997; 81 (1): 350–354. https://doi.org/10.1063/1.364118

[14] R. M. Walser and A. P. Valanju, "Displacement eddy currents in magnetic laminates," in IEEE Transactions on Magnetics, vol. 28, no. 5, pp. 2280-2282, Sept. 1992, doi: 10.1109/20.179469.

[15] A. Geri, A. Salvini and G. M. Veca, "Displacement eddy current computation in magnetic laminates," in IEEE Transactions on Magnetics, vol. 30, no. 2, pp. 1075-1077, March 1994, doi: 10.1109/20.312499.

[16] Kokouvi Etse, Xavier Mininger, "Determination of demagnetizing factors for various geometries using an iterative numerical approach", Journal of Magnetism and Magnetic Materials, Volume 564, Part 2, 2022, 170151, ISSN 0304-8853

[17] Kikuchi, H. & Kamata, Shingo & Nakai, Tomoo & Hashi, Said & Ishiyama, Kazushi. (2015). Influence of demagnetizing field on thin-film GMI magnetic sensor elements with uniaxial magnetic anisotropy. Sensors and Actuators A: Physical. 230. 10.1016/j.sna.2015.04.027.

[18] G. Perrin "Control of the resonance frequency of soft ferromagnetic amorphous thin films by strip patterning", Journal of Applied Physics 81, 5166-5168 (1997) https://doi.org/10.1063/1.365158

[19] F. Fiorillo, Measurement and Characterization of Magnetic Materials, Elsevier Academic Press, 2004, ISBN 0-12-257251-3, page. 31

[20] Stephen Andrilli, Elementary Linear Algebra (Fourth Edition), Academic Press, 2010, ISBN 9780123747518.

[21] Zhang, Daming. (2000). Magnetic skin effect in silicon-iron core at power frequency. Journal of Magnetism and Magnetic Materials - J MAGN MAGN MATER. 221. 414-416. 10.1016/S0304-8853(00)00414-5.